Acta Cryst. (1969). A**25**, 401

Tilt Boundaries in Single Crystals of Cadmium Iodide. I. Formation of Arcs on X-ray Photographs

BY V. K. AGRAWAL AND G. C. TRIGUNAYAT

Department of Physics and Astrophysics, University of Delhi, Delhi-7, India

(*Received* 17 *June* 1968 *and in revised form* 23 *August* 1968)

X-ray oscillation and Laue photographs of solution-grown single crystals of cadmium iodide frequently show extension of the diffraction spots into small continuous or discontinuous arcs. The phenomenon is satisfactorily explained in terms of tilt boundaries formed by vertical alignment of edge dislocations, created during crystal growth. Measurement of arc lengths affords a convenient method for the estimation of dislocation densities inside the crystals. Calculations made on several crystals give the value of dislocation density $\sim 10^5$–10^6 dislocations cm^{-1}.

Introduction

The X-ray diffraction photographs of single crystals of cadmium iodide frequently show streaking and arcing (Trigunayat & Verma, 1962). The streaking phenomenon, in which the reflexions of constant h and k but different l are found to run into each other, is attributed to the stacking faults which occur during the growth of the crystals (Trigunayat, 1966). Silicon carbide and certain other substances also exhibit this effect (Jagodzinski, 1954; Shaw, Steadman & Pugh, 1965). The arcing phenomenon consists of an extension of the diffraction spots into small arcs in a direction perpendicular to the layer lines on the oscillation photographs and was not understood earlier. Now it has been possible to satisfactorily explain the phenomenon in terms of suitable arrangements of dislocations created during crystal growth. The distribution of diffraction spots is more typical on Laue photographs, with each X-ray reflexion extending into either (i) one or more arcs or (ii) a hexagonal ring. The first case is presented in this paper (part I) and the second one is discussed in part II. Recent investigations have shown that the phenomenon is not restricted to cadmium iodide alone. Certain other crystals, *e.g.* PbI_2, $CdBr_2$, *etc.* with layer lattices have also been found to exhibit it. Measurement of arc lengths affords a convenient method of estimating the density of dislocations inside the crystals.

Experimental methods

The crystals were grown from saturated solution. They occurred as hexagonal platelets ranging from nearly $\frac{1}{2}$ mm to 1 mm in size and from nearly 50 microns to 250 microns in thickness and were tested for perfection in a polarizing microscope before X-ray examination. As the crystal were extremely soft, great care was exercised to ensure that they were not deformed while being taken out of the solution or in mounting upon the X-ray camera. The crystals were oscillated about the a axis, so that the c axis was horizontal. The range of oscillation was 15° and was adjusted to lie between 25° and 40°, *i.e.* the angle between the directions of the incident X-ray beam and the c axis varied between 25° and 40°. This range was particularly chosen to record a large number of 01.l reflexions whose l index increased from the centre of the film towards its end. This range was also suited to a separate identification of the upper and lower parts of a crystal since on one X-ray photograph spots were obtained as a result of surface reflexion from one part alone (Chadha & Trigunayat, 1967). The Laue photographs were taken with the X-ray beam incident in the direction of the c axis except in a few cases where this angle was 25°40′, which was particularly suited to record the 00.4n reflexion for an nH polytype, *e.g.* the 00.16 reflexion for the common type 4H. This reflexion, because of its high l value, exhibits a large arcing effect.

The X-ray photographs of all crystals showing the arcing phenomenon were recorded with a camera of radius 3 cm and with a collimator of aperture $\frac{1}{2}$ mm. The size of the focal spot was 1 mm^2.

Experimental results

Nearly one hundred and twenty CdI_2 crystals were subjected to X-ray examination. Almost all of them were found to consist of a mixture of polytypes in syntactic coalescence with each other. As our choice of the range of oscillation (25°–40°) permitted separate identification of the upper and lower parts of a crystal, nearly two hundred and forty oscillation photographs were obtained; the X-ray reflexions were seen to spread into arcs of different lengths on one hundred of these. Laue photographs, when necessary, were also taken. The characteristic features of the various photographs can be described as follows.

(*a*) Some of the Laue and oscillation photographs show clear discrete X-ray reflexions without arcing and streaking (Figs. 1 and 2), *i.e.* each reflexion occurs as a single spot and the neighbouring reflexions do not run horizontally into each other.

(*b*) Some Laue photographs have vertical arcs on the central row, each consisting of two spots lying one above the other and joined by a very faint strip between them (Fig. 3). The corresponding oscillation photograph (Fig. 4) shows vertical arcs on all the layer lines, with the arc length uniformly increasing from the centre of the film towards its end. The spots of l values equal to 14 and 17 (Fig. 3) and of l equal to 16 (Fig. 2) should be particularly observed for the arcing effect in Figs. 3 and 4, as well as in the subsequent Figures, because these spots have high intensities and large arcings. Only one spot is obtained if a small part of the crystal is irradiated by the X-ray beam (Fig. 5). Upon rotating the crystal through 60° about the c axis, so that its other edge becomes the axis of oscillation, the arcs occurring on the central row of the Laue photograph make some angle with it (Fig. 6). The angle increases with the l index. It is $\sim 30°$ for $l=17$. Upon the corresponding oscillation photograph the spots lie one above the other (Fig. 7).

(*c*) The arcs in some of the Laue photographs lie along the central row (Fig. 8; particularly, see the intense $l=16$ spot) *i.e.* the reflexions on this row are line-shaped. Single diffraction spots occur on the corresponding oscillation photograph (Fig. 9). Upon rotating the crystal through 60° about the c axis, the arcs make some angle with the central row which is $\sim 60°$ for $l=16$ (Fig. 10). The corresponding oscillation photograph (Fig. 11) shows arcs perpendicular to the layer lines, each consisting of two spots.

(*d*) On a few Laue photographs, two arcs appear together in place of a single reflexion, giving composite figures of various shapes. Fig. 12 is a representative example, showing fork-shaped reflexions. The two 'prongs' of a 'fork' are nearly equally inclined to the central row.

On all the photographs showing arcing, the lengths of the arcs progressively increase with increasing values of their l indices (Figs. 3, 4, 6, 7, 10 to 12). The syntactically coalesced components pertaining to the upper and lower parts of a crystal have always been found to display different extents of arcing.

Formation of grain boundaries

The solution-grown crystals of cadmium iodide should contain numerous dislocations. Various mechanisms have been suggested for the introduction of dislocations during the growth process, *e.g.* lattice strains due to non-uniform distribution of impurities, convection currents, *etc.* (Trigunayat, 1965). Screw dislocations lying perpendicular to the basal planes and of strengths ranging from nearly fifty Angström units to several thousands of Angström units have been observed in CdI_2 crystals (Forty, 1952; Trigunayat & Verma, 1962). However, as the strength of a unit edge dislocation with a vector of the type $a/3\langle 11\bar{2}0\rangle$ is quite small ($=4{\cdot}24$ Å in CdI_2), edge dislocations should occur far more frequently than screw dislocations, particularly as their formation will be favoured by the crystal structure of cadmium iodide. The structure of cadmium iodide consists of molecular sheets of cadmium and iodine ions piled on top of one another. Each sheet consists of a layer of cadmium ions sandwiched between two layers of hexagonal close-packed iodine ions. The forces within a sheet are purely ionic in nature, giving a strong binding, whereas the layers are held together by weak van der Waals forces of attraction. Therefore, the layers can easily slip under a small stress, giving rise to edge dislocations.

The most likely slip plane in a crystal is always that in which the atoms are closest packed, and slip also takes place in the directions of closest packing. Thus, the most probable slip planes and slip directions in CdI_2 crystals are the $\{0001\}$ basal planes and $\langle 11\bar{2}0\rangle$ directions, respectively. Slip of part of the crystal with respect to the rest along a basal plane will produce an edge dislocation lying in the basal plane having Burgers vector $a/3\langle 11\bar{2}0\rangle$. The edge dislocations of unit strength are most likely to be generated because they need the minimum force for their creation. Besides, the dislocations of strengths greater than unity are unstable as they have high strain energies and can easily decompose into two or more dislocations of unit strength to lower their energies. The existence of dislocations of unit strength is substantiated by experimental observations (Hirsch, 1956). These dislocations cannot dissociate further, except into two half-dislocations such as

$$\frac{a}{3}\langle 11\bar{2}0\rangle = \frac{a}{3}\langle 10\bar{1}0\rangle + \frac{a}{3}\langle 01\bar{1}0\rangle ,$$

i.e. a dislocation on a (0001) plane is transformed into what is called an extended dislocation, which consists of two partials connected by a strip of fault. The partial dislocations repel each other and separate out, but their separation is prevented by the stacking fault energy, since the former is inversely proportional to the latter. Partial dislocations of the above type can also be created independently because the structure of cadmium iodide favours slip in the $\langle 10\bar{1}0\rangle$ directions too, which shifts the atoms in A-positions to B-positions if the atoms in the preceding layer are in C-positions over a part of the slip plane.

Since the stress required for the movement of a dislocation is several orders of magnitude lower than the stress needed to create a dislocation, it follows that the dislocations move freely during the growth of crystals. Because of the asymmetric nature of the interaction between edge dislocations (Cottrell, 1953), the edge dislocations of the same sign become vertically aligned one above the other, leading to the formation of the well-known macroscopically vertical tilt boundaries. A boundary divides the crystal into two blocks tilted relative to one another about an axis lying inside the contact plane of the boundary. As the blocks cannot be produced by fragmentation, a process which may give rise to discontinuities or gaps in the lattice,

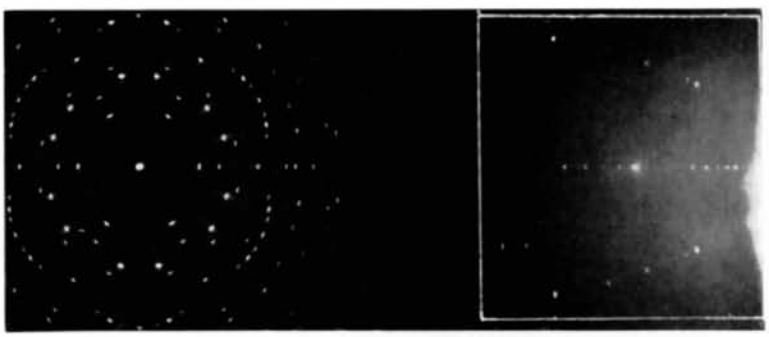

Fig. 1. Laue photograph of crystal No. 1; incident radiation parallel to the *c* axis. *a* axis vertical; Cu white radiation; camera radius 3 cm; polytype 4*H*. The rectangular portion alone, marked by white lines, has been reproduced in the subsequent corresponding Laue photographs.

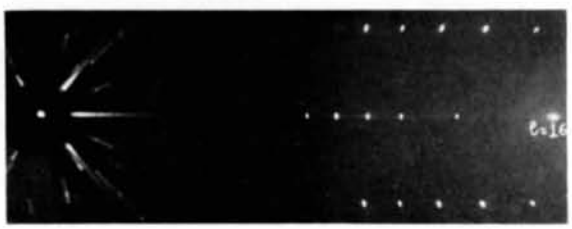

Fig. 2. *a*-axis 15°-oscillation photograph of crystal No. 1; the angle between incident beam and *c* axis varies between 25° and 40°. Cu $K\alpha$ radiation; camera radius 3 cm; polytype 4*H*.

Fig. 3. Laue photograph of crystal No. 2; conditions as in Fig. 1.

[*To face p.* 402

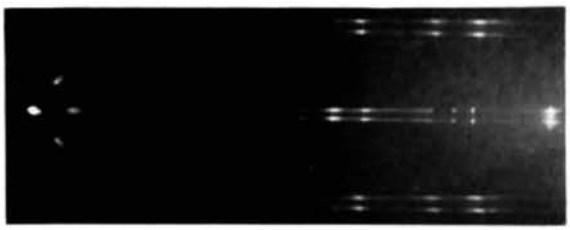

Fig. 4. Oscillation photograph of crystal No. 2. Cu white radiation; other conditions as in Fig. 2.

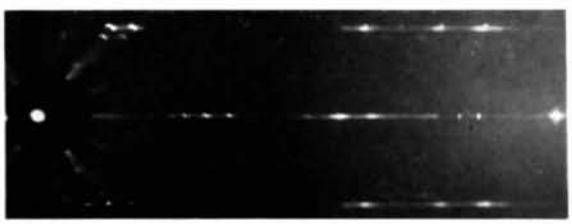

Fig. 5. Oscillation photograph of a portion of crystal No. 2; conditions as in Fig. 4.

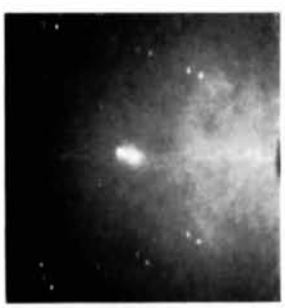

Fig. 6. As Fig. 3 but after rotating the crystal through 60° about the *c* axis.

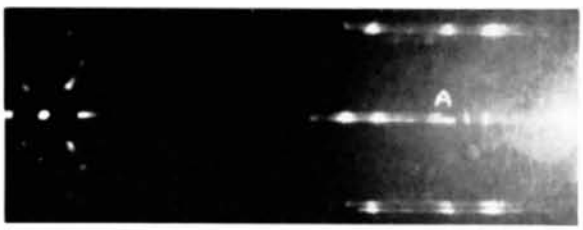

Fig. 7. As Fig. 4 but after rotating the crystal through 60° about the *c* axis.

Fig. 8. Laue photograph of crystal No. 3. Incident radiation makes an angle of 25°40′ with the *c* axis; polytype 4*H*; other conditions as in Fig. 1.

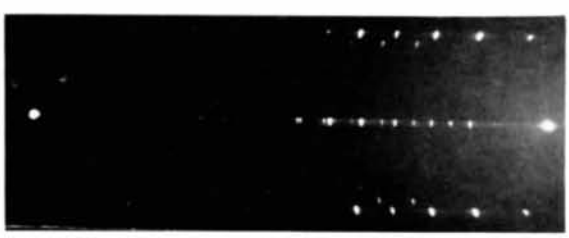

Fig. 9. Oscillation photograph of crystal No. 3. Polytype 4*H*; conditions as in Fig. 4.

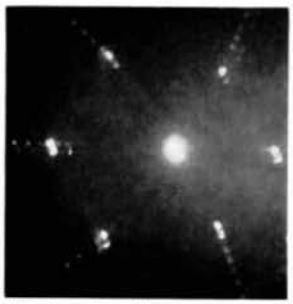

Fig. 10. As Fig. 8 but the crystal was rotated through 60° about the c axis.

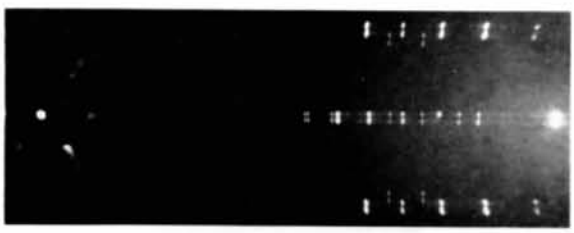

Fig. 11. As Fig. 9 but after rotating the crystal through 60° about the c axis.

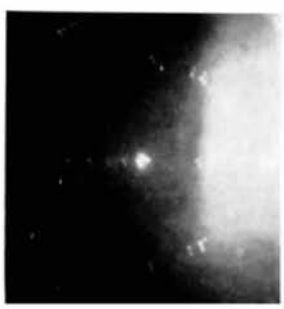

Fig. 12. Laue photograph of crystal No. 4. Polytype $4H$; conditions as in Fig. 1.

[To face p. 403

there is a continuous change of curvature across a tilt boundary from one block to the next. As there are three equivalent directions of closest packing, *viz.* $[11\bar{2}0]$, $[\bar{2}110]$, and $[1\bar{2}10]$, the slip may take place along one, two, or all three of them. The first two cases are discussed in this paper (part I). Slip along all the three possible directions gives rise to ring shaped (hexagonal or trigonal) reflexions, which form the subject matter of the next paper (part II). The less probable slip along the close-packed $\langle 10\bar{1}0\rangle$ directions will generate partial dislocations, which, similarly, can form their own tilt boundaries.

The angle of tilt, θ, is simply related to the dislocation spacing, h, as $\tan \theta/2 = b/2h$ (Cottrell, 1953) where **b** represents the Burgers vector of dislocations lying inside the boundary. For small values of θ, the relationship is given by $\theta = b/h$.

Calculation of the angle of tilt

The angle of tilt, θ, between neighbouring blocks can be evaluated, by measurements on an oscillation X-ray photograph, from a simple relationship that we will now proceed to derive. For hexagonal CdI_2 crystals oscillated about the a axis, reciprocal lattice b^*–c^* nets are horizontal, with an angle between b^* and c^* of 90°. Diffraction spots lying along various horizontal layer lines are obtained by the intersection of the net-points with the sphere of reflexion. The tilt between the two blocks will result in their respective c^* axes also being inclined at the same angle θ to each other, but the angle between b^* and c^* will still remain 90° for either block. The relative positions of the two b^*–c^* nets will depend upon the angle between the axis of oscillation (*viz.* the a axis, which we shall assume to be vertical in the ensuing discussion) and the axis of tilt (lying inside the boundary and parallel to the lines of dislocation). Two orientations of the axis of tilt are possible, *viz.* $[1\bar{1}00]$ and $[11\bar{2}0]$. Since $a=b$ for hexagonal crystal, and therefore any of the 3 pairs of crystal edges can be regarded as the direction of the a axis, six different cases may arise.

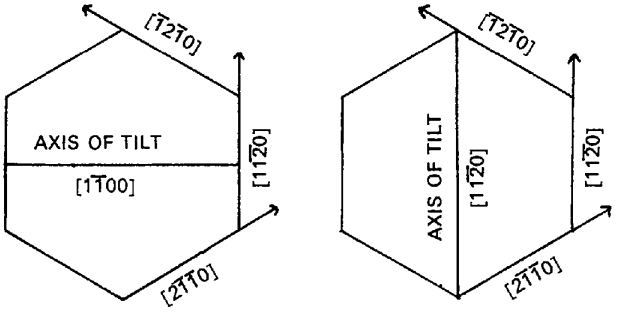

Fig. 13. Possible relative orientations of the a axis with respect to the axis of tilt. c^* is perpendicular to the plane of the paper in both the diagrams.

(i) The axis of tilt lies along $[1\bar{1}00]$ and the a axis along $[11\bar{2}0]$.
(ii) The axis of tilt lies along $[1\bar{1}00]$ and the a axis along $[2\bar{1}\bar{1}0]$.
(iii) The axis of tilt lies along $[1\bar{1}00]$ and the a axis along $[\bar{1}2\bar{1}0]$.
(iv) Both the axes lie along $[11\bar{2}0]$.
(v) The axis of tilt lies along $[11\bar{2}0]$ and the a axis along $[2\bar{1}\bar{1}0]$.
(vi) The axis of tilt lies along $[11\bar{2}0]$ and the a axis along $[\bar{1}2\bar{1}0]$.

The first three cases are depicted in Fig. 13(*a*) and the last three in Fig. 13(*b*). These possibilities will now be examined in detail. It will be noted that case (iii) is identical with case (ii) excepting the case of an opposite orientation of the a axis with respect to the axis of tilt. The same is true for cases (v) and (vi). Hence, cases (iii) and (vi) have not been separately discussed in the following.

Case (i)

The a axis and the axis of tilt are perpendicular to each other in this case, so that the two b^*–c^* nets have a common b^* axis and are rotated about it through the small angle θ. If the b_1^*–c_1^* net be taken to lie in the plane of the paper the b_2^*–c_2^* net lies outside it [Fig. 14(*a*)]. The projection of the latter on the plane of the paper is shown by dotted lines. The plane containing OC_1 and OC_2 is at right angles to OB. Therefore, two corresponding lattice points, P and P', lying along OC_1 and OC_2, respectively, will lie along a small arc subtending an angle θ at the origin O. The intersection of these points with the sphere of reflexion will give rise to an arc-shaped reflexion, consisting of two diffraction spots connected by a strip between them. As indicated earlier, the strip arises from a continuous change in lattice curvature upon going from one block to the next through the intervening boundary, and can have various intensities. Any other X-ray reflexion will be similarly affected.

As seen in Fig. 14(*a*), the length of an arc will depend on its perpendicular distance from OB, *i.e.* on its value of the l index. This distance is $\lambda/c \,.\, l$ and as $\lambda = 1{\cdot}54$ Å for Cu $K\alpha$ radiation and $c = 13{\cdot}67$ Å for the common polytype $4H$, it will be equal to $1{\cdot}54/13{\cdot}67 \,.\, 4/n \,.\, l = x$, say, for an nH-polytype of cadmium iodide. The corresponding length of the arc, like PP', will be equal to $x \,.\, \theta$. Since the sphere of reflexion has a radius equal to unity, the angle subtended by the arc at its centre will be $x\theta$ radians. Therefore, the angle between two reflected beams, one from each block, will be equal to $x\theta$ radians. If r is the camera radius, the length, ε, of the arc recorded on the X-ray film will be given by

$$\varepsilon = r \,.\, x\theta$$

or

$$\theta = \frac{\varepsilon}{r \,.\, x} = \frac{13{\cdot}67}{1{\cdot}54 \times 4} \cdot \frac{n}{l} \cdot \frac{\varepsilon}{r}. \qquad (1)$$

This relation is applicable only to reflexions lying on the zero layer line. For higher layer lines the origins of the corresponding reciprocal lattice nets do not lie on the vertical axis of oscillation. Besides, the ζ-coordinates have also to be taken into account. Hence, the relationships are more complex for these and will not be derived here.

Case (ii)

If the crystal is rotated through 60° about the c axis, the next edge of the crystal becomes the axis of oscillation which will now make an angle of 30° with the axis of tilt; the sizes of the arcs will change. The relative position of two b^*–c^* nets is shown in Fig. 14(*b*). O is the common origin of the two nets. If the b_1^*–c_1^* net is taken to lie on the horizontal plane, taken to be the plane of the paper in the Figure, the b_2^*–c_2^* net lies outside it. The plane containing OC_1 and OC_2 makes an angle of 60° with the vertical plane passing through OC_1. The angle between OC_1 and OC_2 is again equal to the angle of tilt, θ. Thus any two reciprocal lattice points Q and Q' along OC_1 and OC_2, respectively, will lie along an arc subtending the angle θ at the origin. The vertical distance between Q and Q' will be $QQ' \cdot \sin\theta/2\theta \simeq QQ'/2$ (for small values of θ) and the angle between QQ' and its projection on the vertical plane passing through OQ will be ψ, given by $\sin\psi = (\sqrt{3}\sin\theta)/2$, or $\psi \simeq \sqrt{3}\theta/2$ (for small values of θ and ψ). Since both the points Q and Q' essentially correspond to the same lattice plane, the Bragg angle will be the same for both. Therefore during an oscillation, if Q gives rise to a reflexion at an angle φ between the incident X-ray beam and OC_1, a reflexion corresponding to Q' will be obtained at an angle $(\varphi + \psi)$. For the reciprocal lattice points lying along any other lattice row it is necessary to take into account the inclination between the horizontal plane and the plane passing through OB_1 and OB_2. This inclination will depend upon the angle of tilt. To calculate it, consider any two reciprocal lattice points R and R' on OB_1 and

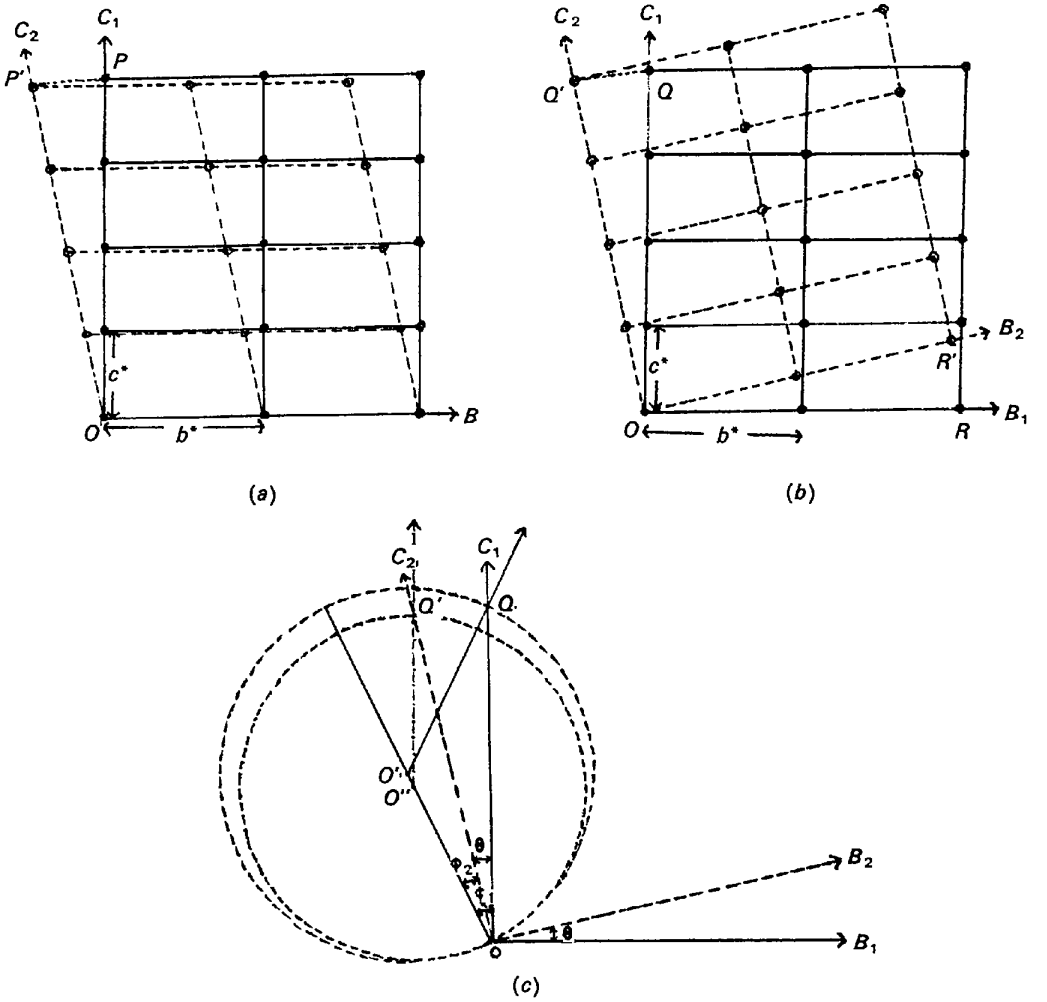

Fig. 14. (*a*) and (*b*). Relative positions of two b^*–c^* nets corresponding to the relevant cases depicted in Fig. 13 (*a*) and (*b*). In both the diagrams, one net, shown by continuous lines, lies in the plane of the paper and the other net, with its projection shown by dotted lines, lies outside it. (*c*) Relative positions of the spheres of reflexion in case (iv).

OB_2, respectively. Since the axis of tilt is inclined at 60° to OB_1, R' will always move along a plane inclined at 30° to OR as θ varies. The angle α between the horizontal plane and the plane passing through OR and OR' is evaluated to be equal to $\tan^{-1}(\frac{1}{2}\tan\theta/2) \simeq \theta/4$ (for small values of θ). The angle between OR and the projection of OR' on the horizontal plane can similarly be calculated to be equal to $\tan^{-1}\frac{2\sqrt{3}\tan\theta/2}{2-\tan^2\theta/2} \simeq \sqrt{3}\theta/2$ (for small θ's) and the vertical distance between R and R' to be equal to $\sqrt{3}/2 \,.\, OR \,.\, \sin^2\theta/2$. For small θ values this vertical distance can be neglected so that OB_1 and OB_2 can be taken to lie on the same horizontal plane and the angle between them taken to be equal to $\sqrt{3}/2\theta$. Thus the arc lengths will directly depend on the values of the l index as in the previous case. There are two points of difference between cases (i) and (ii). (*a*) The arc lengths for the same reflexion will be in the ratio 2:1 in the respective cases and (*b*) the two reciprocal lattice points pertaining to a pair of blocks will give rise to reflexions at the same angle φ between the X-ray beam and OC_1 in case (i), and at different angles φ and $(\varphi+\sqrt{3}/2\theta)$ in the case (ii).

Case (iv)

The *a* axis and the axis of tilt now point in the same direction. The relative positions of the two b^*–c^* nets can be represented as in Fig. 14(*b*), provided that they are now taken to lie, and to be rotated through the angle θ, in the same plane, *viz.* the plane of paper. Two lattice points, like Q, Q' in Fig. 14(*b*) will give rise to reflexions at angles φ and $(\varphi+\theta)$, respectively, between the X-ray beam and OC_1. Since both the nets lie on the same plane, the reflexions from both the points will overlap. Therefore there will be no arcing on the oscillation photograph. The angle of tilt can be determined from the Laue photograph, in which Q, Q' will give rise to reflexions corresponding to two different wave lengths satisfying the Bragg condition for two different angles φ_1, φ_2 [Fig. 14(*c*)]. The difference between φ_1 and φ_2 will be equal to the angle of tilt, θ. Therefore, the angle between two reflected beams will be equal to 2θ. If the Laue photograph is also obtained on a cylindrical film, of radius r, the arc will lie along the central row and its length will be given by

$$\varepsilon = r \,.\, 2\theta$$

or

$$\theta = \varepsilon/2r \,. \qquad (2)$$

Case (v)

The angle between the *a* axis and the axis of tilt is 60° in this case. The arc lengths can be evaluated by a similar method as given in case (ii). Here the plane containing OC_1 and OC_2 is inclined at 30° to the vertical plane passing through OC_1 [Fig. 14(*b*)]. Therefore the vertical distance between Q and Q' will be $\sqrt{3}/2QQ' \,.\, \sin\theta/\theta \simeq \sqrt{3}/2QQ'$, and the angle between OQ' and its projection on the vertical plane containing OQ will be $\sin^{-1}(\sin\theta/2) \simeq \theta/2$. For small values of θ, OB_1 and OB_2 are again taken to lie on the same plane as in case (ii) and to make an angle $\sim\theta/2$ between themselves. Thus the two reciprocal lattice points Q and Q', will give rise to reflexions at angle φ and $(\varphi+\theta/2)$, respectively, between the X-ray beam and OC_1. The arc lengths for the same reflexion will be in the ratio $1:\sqrt{3}/2$ in cases (i) and (v), respectively. Accordingly, the angle of tilt, θ, can again be found from equation (1), provided the observed arc lengths are multiplied by $2/\sqrt{3}$.

Discussion

The experimental findings, described earlier, are found to agree fully, both qualitatively and quantitatively, with the theoretical deductions made in the preceding section about the origin of the arcing effect and the estimation of the angle of tilt for the various cases. For clarity of presentation, the results are separately discussed for each case.

Case (i)

In Fig. 3, which is the Laue photograph of crystal No. 2, each arc consists of two spots joined by a strip perpendicular to the central row, showing that the crystal is divided into two blocks tilted with respect to one another about an axis perpendicular to the *a* axis (*cf.* Fig. 1). As mentioned earlier, the strip arises from the continuously distorted region between the two blocks. If only one block is irradiated by the X-ray beam, only one spot, instead of an arc, is obtained (Fig. 5). The corresponding oscillation photograph (Fig. 4; *cf.* Fig. 2) shows vertical arcs. The range of oscillation being such that the l index of a reflexion uniformly increases with its ξ value, the arc length progressively increases from the centre of the photograph towards its end. The same does not happen in those ranges in which the l indices of the spots do not continuously increase with their ξ values. The angle of tilt can be easily calculated by measuring the length of any arc in Fig. 4 and substituting the value in equation (1).

Case (ii)

Upon rotating the same crystal through 60° about the *c* axis, the arcs on the central row make the angle $\tan^{-1} x/2\sqrt{3}$ with the axis, which is $\sim 30°$ for $l=17$ in the Laue photograph (Fig. 6), since the axis of tilt now makes an angle of 30° with the *a* axis. In Fig. 6, the upper spot is seen to split further into two close spots, revealing the existence of a sub-boundary in the corresponding block. The mutual vertical alignment of the two spots shows that the axis of tilt inside this block is perpendicular to the *a* axis. During oscillation (Fig. 7), all the three spots come one above the other and if the range of oscillation for one block is 25° to 40°, it is $(25° \pm \sqrt{3}/2\theta)$ to $(40° \pm \sqrt{3}/2\theta)$ for the other. At point A in Fig. 7, it is seen that the Laue streak joining the lower spots on the zero layer line is longer

than those joining the upper spots, proving that the two corresponding blocks have different ranges of oscillation. A comparison of Figs. 4 and 7 shows that the arc lengths for each reflexion are halved in the latter photograph, as estimated theoretically.

Case (iv)

Line-shaped reflexions, consisting of two or more spots connected by a strip, are obtained on the central row of the Laue photograph if the axis of tilt is parallel to the *a* axis. The tilt boundary in this case is made up of partial dislocations generated by slip in one of the $\langle 10\bar{1}0 \rangle$ directions. A Laue photograph was taken at an angle equal to 25°40′, between the X-ray beam and the *c* axis, for recording the (00.16) reflexion, which is quite isolated from the other reflexions (Fig. 8). It is seen to consist of two spots lying along the central row, one of which is far more intense and bigger in size than the other. During oscillation, the two blocks successively reflect to a single common position. Hence, single, discrete reflexions, without arcing, are obtained all over the photograph (Fig. 9). The angle of tilt can be determined from equation (2).

Case (v)

The Laue photograph (Fig. 10) of the same crystal, *viz.* No. 3, obtained by rotating it through 60° in one direction, shows the arcs on the central row to have become obliquely oriented at about 60° (for $l=16$) with respect to it, because the axis of tilt is now inclined to the *a* axis. The two blocks now reflect to different positions on the oscillation photograph (Fig. 11), which therefore shows the arcing phenomenon, with each arc consisting of two spots.

Composite figures

Fig. 12, which is the Laue photograph of crystal No. 4, shows fork-shaped reflexions on the central row, with the two 'prongs' of a 'fork' symmetrically inclined to the row. The angle of inclination is about 60° for the reflexion $l=17$. These are due to the combined effect of two tilt boundaries of partial dislocations, both inclined at 60° to the *a* axis but in opposite directions (Fig. 15). It is also feasible that *XOY* (Fig. 15) represents a composite boundary of extended dislocations having component half-dislocations along *OX* and *OY*, respectively. The Laue photograph (not reproduced) obtained on irradiating only a part of the crystal showed only one prong of each fork. The oscillation photograph of the crystal shows vertical arcs, with each arc consisting of four spots. It has not been reproduced here.

Composite reflexions of various other shapes, *e.g.* cross-shaped, square-shaped, semi-elliptical, *etc.*, have also been observed, but only rarely. They all can be similarly explained as a combined effect of various arrangements of dislocation boundaries.

The upper and lower faces of a crystal have always been found to display different degrees of arcing. In many cases, it is also found that one of them gives clear, discrete reflexions, without any arcing whatsoever. Usually the lower face shows more arcing than the upper one. It follows that the dislocations are not created at a uniform rate during crystal growth. Their rate of formation is rapid in the initial stages, when the growth rate itself is high, and slows down towards the end.

The shapes and relative sizes of the spots on an arc are usually not the same (Figs. 6, 8, 10 to 12) which can be satisfactorily explained by taking account of the influence of dislocations inside the blocks. The dislocations of either sign in the blocks are arranged to form subsidiary blocks separated by sub-boundaries. But the angles of tilt are very small as compared to the angles between the blocks themselves. The tangential breadth of a spot is the measure of the average

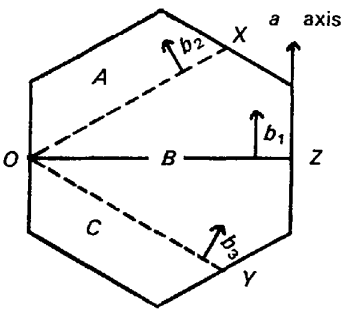

Fig. 15. Division of a crystal into 3 blocks *A*, *B*, *C* by tilt boundaries of partial dislocations, of Burgers vectors $\mathbf{b}_2$ and $\mathbf{b}_3$, along *OX* and *OY*. A unit dislocation, of Burgers vector $\mathbf{b}_1$, along *OZ* can dissociate into these two components.

Table 1. *Densities of dislocations in tilt boundaries*

Specimen number	Arc length for (00·16) reflexion (cm)	Angle of tilt	Burgers vector (Å)	Density of dislocations (dislocations cm^{-1})
1	0·168	1°47′	4·24	$7{\cdot}33\times10^5$
2	0·165	1°35′	4·24/√3	$1{\cdot}12\times10^6$
3	0·242	2°34′	4·24	$1{\cdot}06\times10^6$
4	0·410	4°21′	4·24	$1{\cdot}79\times10^6$
5	0·068	0°43′	4·24	$2{\cdot}97\times10^5$
6	0·102	1°05′	4·24	$4{\cdot}45\times10^5$
7	0·212	2°15′	4·24	$9{\cdot}25\times10^5$
8	0·170	1°37′	4·24/√3	$1{\cdot}16\times10^6$
9	0·238	2°32′	4·24	$1{\cdot}04\times10^6$
10	0·104	1°06′	4·24	$4{\cdot}54\times10^5$

density of dislocations within the block. The radial breadth of the spots results from streaking, seen on many photographs (Figs. 4, 5, 7, 9, 11), which has its origin in the stacking faults randomly occurring in the structure during crystal growth (Trigunayat, 1966).

Density of dislocations

If h is the spacing between dislocations in a boundary, the density of dislocations, ϱ, is equal to $1/h$. For small values of θ, $h=b/\theta$. Therefore,

$$\varrho=\theta/b \text{ dislocations cm}^{-1}.$$

The Burgers vector of $a/3\langle 11\bar{2}0\rangle$ dislocations is 4·24 Å and of $a/3\langle 10\bar{1}0\rangle$ dislocations is $4{\cdot}24/\sqrt{3}$ Å in CdI_2 crystals.

Thus the density of dislocations in the boundaries depends directly upon the angle of tilt and hence upon the arc length. It is found to be of the order of 10^5–10^6 dislocations cm^{-1}. The values calculated for a few crystals are listed in Table 1.

The dislocations inside the crystal are considered to be located in the boundaries and inside the blocks, but the number of dislocations inside the block is much less than in the boundaries because the tangential breadth of a spot is generally observed to be much smaller than the arc length.

References

CHADHA, G. K. & TRIGUNAYAT, G. C. (1967). *Acta Cryst.* **22**, 573.

COTTRELL, A. H. (1953). *Dislocations and Plastic Flow in Crystals*. Oxford: Clarendon Press.

FORTY, A. J. (1952). *Phil. Mag.* **43**, 377.

HIRSCH, P. B. (1956). *Progress in Metal Physics*. Vol. 6. London: Pergamon Press.

JAGODZINSKI, H. (1954). *Neues Jahrb. Mineral.* **3**, 49.

SHAW, R., STEADMAN, R. & PUGH, P. D. (1965). *Z. Kristallogr.* **122**, 237.

TRIGUNAYAT, G. C. (1965). *Z. Kristallogr.* **122**, 463.

TRIGUNAYAT, G. C. (1966). *Nature, Lond.* **212**, 808.

TRIGUNAYAT, G. C. & VERMA, A. R. (1962). *Acta Cryst.* **15**, 499.

Acta Cryst. (1969). A**25**, 407

Tilt Boundaries in Single Crystals of Cadmium Iodide. II. Formation of Closed Rings on X-ray Photographs

BY V. K. AGRAWAL AND G. C. TRIGUNAYAT

Department of Physics and Astrophysics, University of Delhi, Delhi-7, India

(*Received* 17 *June* 1968 *and in revised form* 23 *August* 1968)

The X-ray a-axis Laue photographs of single crystals of cadmium iodide grown from solution sometimes show closed rings of various shapes, *viz.* hexagonal, trigonal, *etc.* and of various sizes, corresponding to each X-ray reflexion. They have been satisfactory explained in terms of the formation of more than two tilt boundaries of dislocations during crystal growth. The boundaries result from a vertical alignment of triple nodes of dislocations created by simultaneous slip along close-packed directions. In most cases the slip is confined to the basal planes and occurs at regular intervals.

Introduction

The oscillation and Laue photographs of CdI_2 crystals showing arcing, which consists of an extension of diffraction spots into small arcs, have been discussed in detail in part I (Agrawal & Trigunayat, 1969). This part includes the crystals which show closed rings of various shapes, *viz.* hexagonal, trigonal, *etc.* and of various sizes, on their Laue photographs. Their formation can be adequately explained by postulating the creation of more than two tilt boundaries of dislocations. Similar observations have also been made in single crystals of cadmium bromide grown from solution and will be described later.

Experimental methods

The methods employed for growing the crystals, selecting them, and subjecting them to X-ray examination were the same as described in part I.

Formation of tilt boundaries

Slip along one, or at the most two, close-packed directions at a time was considered in part I. We now consider the possibility of slip simultaneously taking place along the third direction as well. A unit slip on the (0001) basal plane along one of the closest-packed directions, *viz.* $[11\bar{2}0]$, $[\bar{2}110]$, $[1\bar{2}10]$ and their negatives,